

Received August 2, 2020, accepted August 9, 2020, date of publication August 18, 2020, date of current version August 31, 2020.

Digital Object Identifier 10.1109/ACCESS.2020.3017458

A Life Cycle-Cost Analysis of Li-ion and Lead-Acid BESSs and Their Actively Hybridized ESSs With Supercapacitors for Islanded Microgrid Applications

MARYAM TORKASHVAND¹, ABOLFAZL KHODADADI²,
MEHRDAD BAGHERI SANJAREH³, AND MUHAMMAD H. NAZARY⁴

¹Department of Electrical and Computer Engineering, Islamic Azad University Science and Research Branch, Tehran 1477893855, Iran

²Division of Electric Power and Energy Systems, KTH Royal Institute of Technology, 1004483 Stockholm, Sweden

³Department of Electrical Engineering, Shahid Beheshti University, Tehran 1983969411, Iran

⁴Center of Excellence in Power Systems, Department of Electrical Engineering, Amirkabir University of Technology, Tehran 1983969411, Iran

Corresponding author: Maryam Torkashvand (dr.torkashvand@gmail.com)


ABSTRACT The combination of supercapacitors (SCs) with Li-ion Batteries (LIBs) and Lead-Acid Batteries (LABs) as hybrid ESSs (HESSs) have widely been proposed for Microgrid (MG) applications. The SCs of HESSs eliminate the stress of surge currents on LIBs and LABs, which increases their life cycles, and decreases their life cycle costs and hence decreases the HESSs operational costs. However, the active topology of HESS, which is the most commonly used configuration, requires an extra SC and an extra DC/DC converter in comparison to the Battery Energy Storage (BESS) topology, which increases the HESS capital cost. This paper tries to investigate that the hybridization of LABs and LIBs with SCs is economically effective or not for applications in islanded MG. In this regard, an energy management and frequency control (EMFC) scheme is proposed for the operation of MG in islanded mode. Using the simulations of the proposed EMFC scheme for islanded MG, the size of main components of LIB ESS (LIBESS), LAB ESS (LABESS), LIB-SC HESS (LISHNESS) and LAB-SC HESS (LASHNESS) are calculated. The numerical results show that for a 10-year period operation in islanded MG, the LISHNESS and LASHNESS impose less cost than LIBESS and LABESS. Also, the LISHNESS is cheaper (almost 11%) than LASHNESS.

INDEX TERMS Microgrid, li-ion battery, lead-acid battery, supercapacitor.

I. INTRODUCTION

Integration of micro-sources and energy storage systems can construct a power grid so called microgrid (MG) to meet the demands, which can be operated in both grid-connected and standalone (islanded) modes. In the grid-connected mode, the utility grid should guarantee the demand-supply balance in the MG, and therefore the frequency in this mode is maintained on its nominal value [1], [2]. The main objective of MG operator in the grid-connected mode is to minimize power import from the grid by maximum utilization of renewable distributed generators (DGs) and coordinated control of ESSs and loads, while minimizing power losses and use of fuel-based DGs [3]. In case of disturbances or failure in the main grid, the MG shifts its operation to islanded mode to ensure system stability. In the islanded mode, the MG may

suffer from the imbalance between the demand and supply [4], and as the capacity of DGs is limited, they may not be able to supply the loads during some periods. Therefore, the primary concern is to meet demand by available resources [5]. The intermittent nature of renewable DGs makes the task of maintaining the supply-demand balance even harder in islanded mode, which necessitates the installation of an ESS for this task [6]–[8]. Battery ESSs (BESSs) are accepted as one of the most important and efficient ways to maintain reliable energy supply. Among various battery technologies, the Lead-Acid batteries (LABs) are the most commonly used for grid-based applications [9]. Also, the research in [10] has referred to the Lithium-Ion Battery (LIB) as the most promising battery technology. Therefore, in this paper, both LIBs and LABs are considered for microgrid applications in islanded mode. In [11], Lithium-ion battery (LIB) is used for peak shaving and load leveling. In a standalone MG, the Lead-Acid batteries (LABs) are used for energy

The associate editor coordinating the review of this manuscript and approving it for publication was Jun Shen .

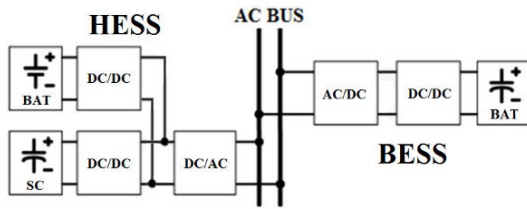


FIGURE 1. BESS/HESS configuration.

management and compensating supply-demand mismatch [12], [13]. The authors of [4], [14] investigated the application of LIB/LAB ESSs (LIBESS/LABESS) for frequency regulation of islanded MGs, respectively.

In various studies, it has been stated that fast power regulations and high-power applications like frequency regulation shorten the life of LIBs and LABs [15], [16]. In this regard, the combination of supercapacitors (SCs) with batteries as hybrid ESSs (HESSs) have been proposed to reduce the stress of surge currents [17]. For this purpose, SCs are used to handle sudden variations of load demand and fast power fluctuations while batteries are used to just respond to slow power fluctuations [18], [19]. In [20], the SC is used to enhance the service life of the Lead-acid battery in a standalone photovoltaic-battery power systems by mitigating life-limiting factors such as current fluctuations and surge currents. In [21], an energy management scheme is proposed to maintain power balance using a HESS in an MG with renewable generation that due to the absence of dispatchable DGs, the battery might be overcharged/overdischarged. To avoid these conditions, the authors have proposed to disconnect loads and decrease photovoltaic (PV) power generation below maximum power point in shortage and surplus scenarios of power generation, respectively. In this study, the proposed energy management scheme uses the coordination of dispatchable DGs and the battery to prevent load shedding and also to ensure that PVs always operate at maximum power point. In [22], the LIB-SC HESS (LISHESS) results in 19% increase in LIBs lifespan. Similarly, the authors of [23] discovered that the LAB-SC HESS (LASHESS) results in 30% increase in LABs lifespan. The increase in lifespans of LIBs and LABs result in less operating cost.

Fig. 1 shows the topology of a BESS and a HESS. Among different HESS configurations, the active topology is the most commonly used configuration [24]. It can be observed that the HESS requires an extra SC and an extra converter, which increases HESS cost. In other words, as the HESS operation cost decreases, the HESS capital cost increases. Furthermore, in [25] the authors stated at least 50% life extension is necessary to make hybridization with the SCs cost effective for application in the electric vehicles.

The installation of an ESS with random/inappropriate size can be problematic such as imposing extra cost to the MG. In order to minimize total cost of BESS, the authors of [26], [27] have determined the minimal size of battery including its rated power and rated capacity for islanded operation of MG for a limited period using short-term frequency

regulation studies. However, the authors have not clearly explained how the dimensions of the battery especially its rated capacity is determined. Considering that maintaining balance in energy demand and supply in islanded MG is the priority [5], long-term energy management studies are required to determine the required energy storage capacity for this task, which are not performed in [26], [27]. In this study, both short-term frequency regulation and long-term energy management studies are conducted to determine the required power rating and capacity of the ESS elements.

In this paper, a life cycle-cost analysis is performed to determine whether the active hybridization of LIBs and LABs with SCs is cost effective or not for MG applications. An energy management and frequency control (EMFC) scheme is proposed for MG operation in islanded mode, which ensures the demand-supply balance and maintenance of frequency deviation within allowable limits using ESS elements with minimal size. Using the proposed EMFC scheme, the size of components of LIBESS, LABESS, LISHESS and LASHESS is determined. Then, their costs are evaluated and compared for a 10-year period. The main contributions of this paper are:

- To the best of the authors' knowledge, a similar research has never been conducted to economically analyze two BESS technologies and their actively hybridized ESSs with SCs for islanded MG applications.
- Unlike [26], [27] that proposed a vague approach based on frequency regulation studies, here, a comprehensible approach is proposed based on both short-term frequency regulation and long-term energy management studies to determine dimensions of the battery and the SC for the islanded operation of the MG.
- The proposed EMFC uses the coordination of DGs and battery in minimization of the required battery capacity for maintaining the demand-supply balance. The MG frequency is also kept within permitted operational limits using the optimal tuning of frequency controllers of battery/SC.
- Introducing the procedure and formulae for cost calculation of four commonly used and studied ESS technologies.

The general overview of the sections, simulations, figures, tables and their relations are shown in Fig. 2.

II. PROPOSED EMFC SCHEME

The utility grid guarantees the demand-supply balance in the MG in the grid-connected mode, and thus, the frequency can be maintained in an acceptable range; though, in the islanded mode, the MG may experience fast frequency deviations due to the intermittent nature of renewable sources, load variations and etc. The frequency of the islanded MG can be governed by (1)[7]:

$$\frac{df}{dt} = \frac{f_0}{2H_{MG}} (P_G - P_L) \quad (1)$$

where, f and f_0 is the MG frequency and the MG nominal frequency respectively. Also, H_{MG} is the MG total inertia, P_G ,

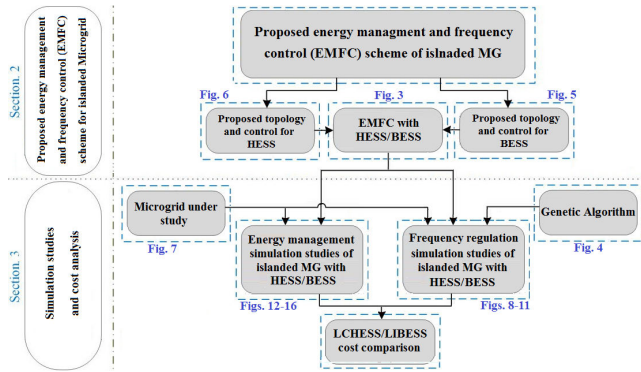


FIGURE 2. The schematic diagram of the paper sections and their connections.

and P_L are the total power generation and consumption of the MG, respectively.

In islanded mode, the MG microsources are responsible for maintaining the demand-supply balance. Considering inherent slow response characteristics, the slow responding DGs are incapable of handling fast power regulations. However, the total capacity of DGs can supply the MG base load, but they cannot supply the peak load. Therefore, the installation of an ESS is necessary for fast transient power regulations and energy management during the peak-load period. Based on (1), the EMFC diagram of the islanded MG with coordinated control of an ESS and DGs is shown in Fig. 3. All the DGs have outputs representing the power generation of the DG while only dispatchable DGs have inputs to receive the power setpoint. Renewable sources like PVs are assumed to be controlled to produce their maximum power. As far as the balance between consumption and generation is maintained, the frequency is stable and remains in acceptable range.

The proposed frequency control consists of two stages: 1) primary frequency control (PFC) by the ESS using a proportional controller, which is denoted by K_1 , 2) Secondary frequency control (frequency restoration) by dispatchable DGs using an integral controller, which is denoted by K_2 . Regarding the PFC using LASHCESS and LISHESS, the interception of the frequency deviation is handled by the SC. It responds to high-frequency components of MG frequency deviations using a high-pass filter. By doing this, fast power regulations are diverted to the SC. This is while the battery responds to low-frequency components of MG frequency deviations and deals with slow power regulations using a low-pass filter and a proportional controller, which is denoted by K_3 .

In case the DGs reach their maximum power, the battery also participates in the frequency restoration using an integral controller, which is denoted by K_4 . Another integral controller, which is denoted by K_5 , is also used to restore the battery power to zero, if the DGs are not generating their maximum power. In addition, an integral controller, which is denoted by K_{SOC} , is used to control DGs power to discharge/charge the battery to maintain the (SOC_{BAT}) at reference value (SOC_{BAT}^{ref}).

The acceptable limits in frequency deviations of an islanded MG is $\pm 1\%$ of the rated value [28]. This paper proposes a novel approach for maintaining the MG frequency within permitted operational limits. By increasing and decreasing K_1 , the rate of power injection for frequency interception increases and decreases, respectively; the higher rate of the power injection/absorption, the less frequency deviation. Fig. 4 shows the tuning process of the K_1 by Genetic Algorithm (GA), which ensures enough

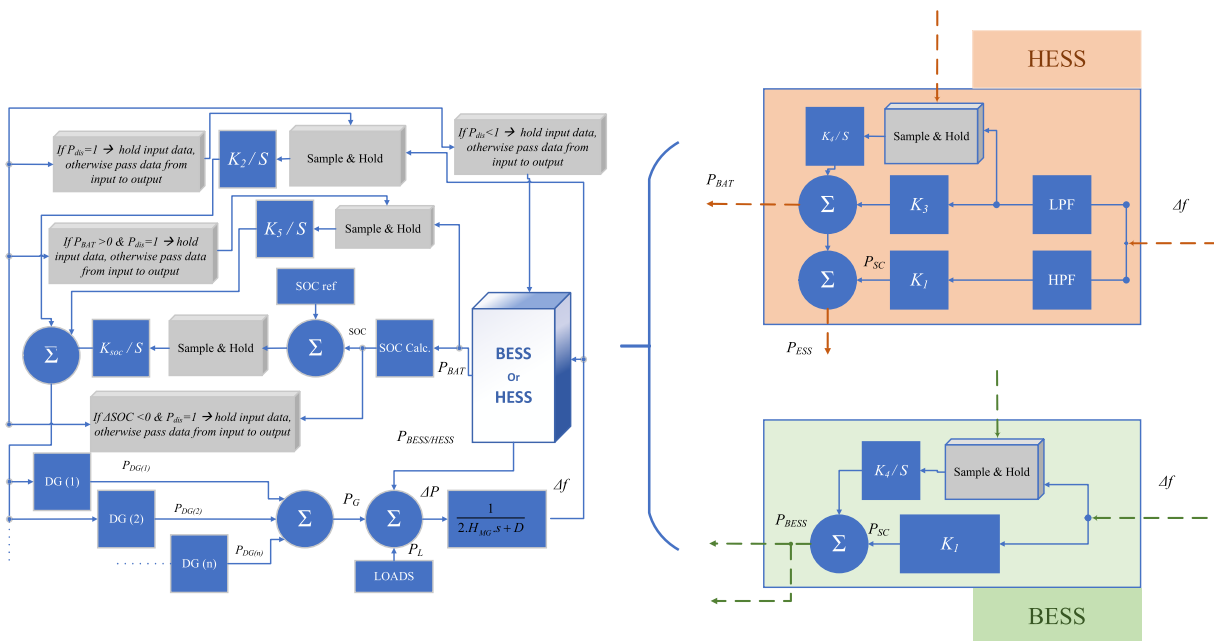


FIGURE 3. EMFC diagram of islanded MG.

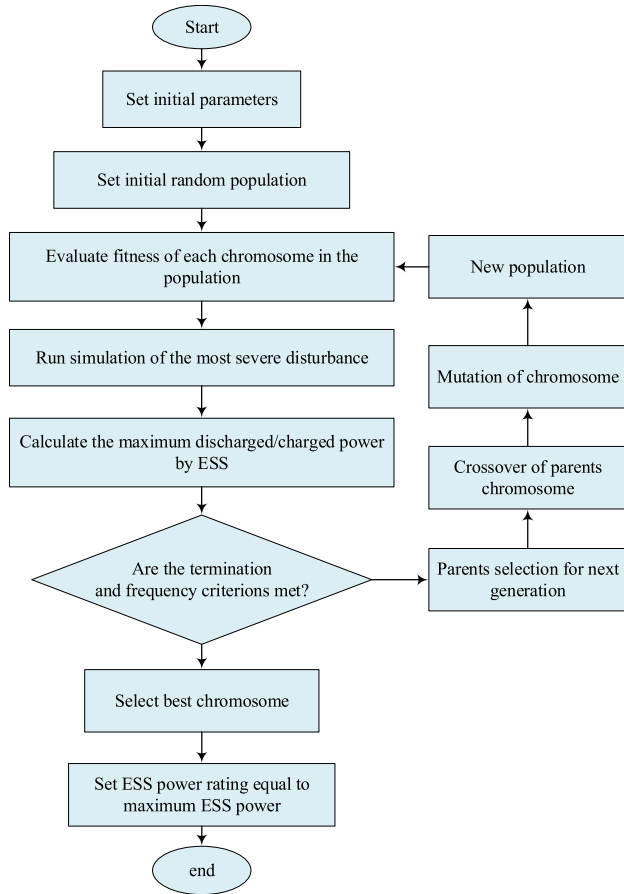


FIGURE 4. Tuning process of PFC controller of ESS.

power is injected/absorbed to maintain the frequency within the permitted limits when the most severe disturbance occurs [29]–[31].

In fact, the genetic algorithm is used just once to determine the value of frequency controllers. In real-time operation, the frequency controllers, which are optimally determined

by the GA, are used to handle frequency control. The most severe frequency disturbance is considered so that the MG frequency remains within allowable limits in any less severe disturbances as well. The power rating of the ESS elements participating in PFC is determined based on the maximum power injection/absorption.

The ESS control strategy for energy management in islanding mode is charging during off-peak period, and discharging during peak hours. The mid-summer day, which has the heaviest daily load profile, is chosen as the worst case for ESS capacity sizing. If the BESS can manage power balance in this case, it certainly can take care of the MG energy management in less severe cases like any other days in a year as well.

A. CONFIGURATION OF BESS AND HESS FOR EMFC SCHEME FOR PFC

Fig. 5 shows the components, topology and control system of a BESS, which is connected to the MG. It mainly consists of a battery stack, a bidirectional DC/DC converter, a bidirectional three-phase inverter and filters. In addition, current and voltage transformers are used to take current and voltage samples from the inverter output. The phase-locked loops (PLLs) are also used to determine the phase angle and frequency.

The discharge/charge control of the battery through the control of the DC/DC converter has been completely described in [32]. The power reference (P_{batref}) determines the required power injection/absorption by the battery. In the grid-connected mode, the MG management center determined the setpoint for the battery power. However, in the islanded mode, P_{batref} is defined by a MG proportional-integral (PI) controller. The error signal of integral and proportional controllers and the actual battery power determine P_{batref} . If the DGs reached the maximum power generation, the integral controller would be blocked and only the proportional controller would be functional.

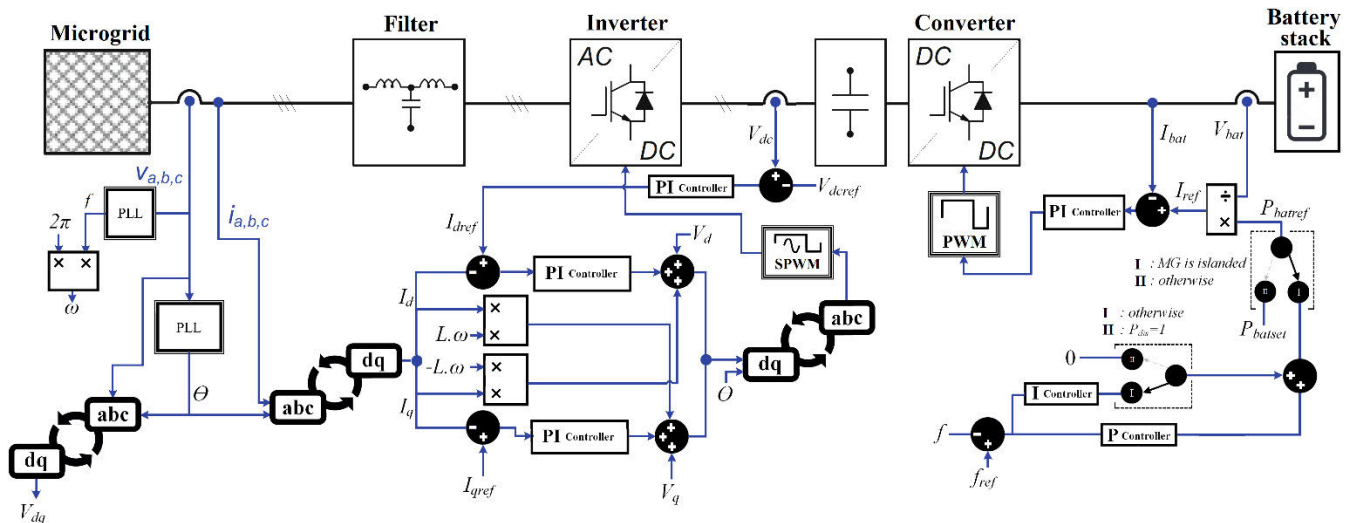


FIGURE 5. BESS connected to MG; components and control system.

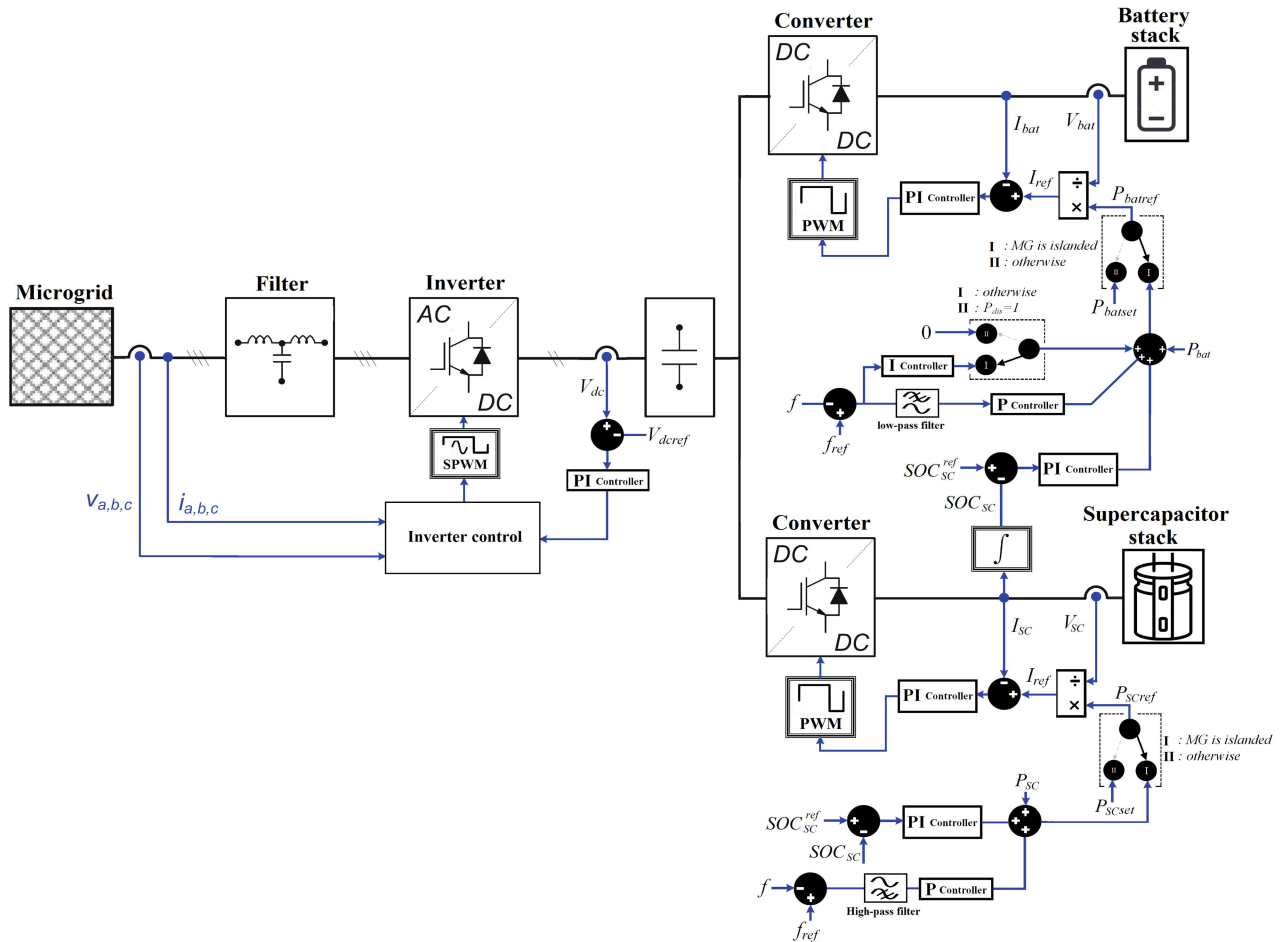


FIGURE 6. HESS connected to MG; its components and its control system.

The inverter controller is the conventional dq current controller, completely discussed in [7]. I_{dref} and I_{qref} determine the output active and reactive powers of the inverter. The voltage of the DC link (V_{DC}) between the converter and the inverter is maintained at a reference level (V_{DCref}). To realize this task, a PI controller is used to regulate I_{dref} . For discharging the battery energy to the MG, the converter discharges the energy of the battery into the DC link capacitor (C_{DC}), which results in an increase in V_{DC} . The inverter controller tries to keep V_{DC} at V_{DCref} . Therefore, the inverter discharges the charged capacitor energy to the MG. For charging the battery from the MG, the converter takes energy from C_{DC} , which causes the V_{DC} to decrease. The inverter controller tries to keep the V_{DC} at V_{DCref} . Therefore, the inverter charges the discharged capacitor energy from the MG. In this paper, I_{qref} is set to zero to maintain unity power factor [7].

Fig. 6 shows the topology, components and control system of a HESS, which is connected to the MG. The HESS consists of two ESS elements that in this paper one of them is the SC and the other is a battery, which is either an LAB or an LIB. Each of them is connected to a separate converter. Some major parts of the HESS is the same as BESS like the converters and the battery discharge/charge controller. The frequency controller of the battery in HESS is the same BESS except

that the battery frequency controller in HESS just responds to low-frequency components of the MG frequency using a low-pass filter. The SC just responds to the high-frequency components using a high-pass filter and does not participate in frequency restoration. The time constants of the high-pass and low-pass filters (T) are chosen 1.5 sec as proposed in [13]. In addition, two PI controllers are added in the power reference controller of the battery and SC. Using these PI controllers, if the SOC_{SC} is lower than SOC_{SC}^{ref} , the battery discharge its energy to the SC through the DC link to charge the SC. If the SOC_{SC} is higher than SOC_{SC}^{ref} , the SC discharge its energy to the battery. This process is continuously executed to maintain the SOC_{SC} at SOC_{SC}^{ref} . It can be seen that the topology and control of HESS is more complex than that of BESS.

B. COST FORMULATION OF BESS AND HESS FOR PRIMARY FREQUENCY CONTROL

The BESS mainly consists of a battery stack, a converter, and an inverter, its cost can be calculated using (2):

$$C_{BAT} = (RC_{BAT} \cdot BC_{BAT}) + (RP_{Con} \cdot BC_{Con}) + (RP_{Inv} \cdot BC_{Inv}) \quad (2)$$

where, BC_{Con} is the base cost (\$/kW) of the bidirectional DC/DC converter. RP_{Con} is the rated power (kW) of the

bidirectional DC/DC converter. RP_{Inv} and BC_{Inv} are the rated power (kW) and base cost (\$/kW) of the bidirectional Inverter. RC_{BAT} and BC_{BAT} are the rated capacity (kWh) and base cost (\$/kWh) of the LIB/LAB. The rated capacity of the LIB/LAB stack can be calculated using (3), based on its maximum discharged energy (E_{maxDis}^{BAT}) in the EMFC studies.

$$RC_{BAT} = \frac{E_{maxDis}^{BAT}}{\eta_{Inv} \cdot \eta_{Conv}} \quad (3)$$

The cost of the LIB with 6000 life cycles is 1000 \$/kWh [33]. The cost of an LAB cell with 2000 life cycles is 600 \$/kWh [34]. Considering one discharge/charge cycle per day [35], the BC_{LIB} for LAB and LIB can be calculated for a 10-year period:

$$\begin{aligned} BC_{BAT}(LIB) &= \frac{1000\$}{6000 [life_cycles]} \times 3650cycles \\ &\cong 608.34 \text{ \$/kWh} \end{aligned} \quad (4)$$

$$\begin{aligned} BC_{BAT}(LAB) &= \frac{600\$}{2000 [life_cycles]} \times 3650cycles \\ &\cong 730 \text{ \$/kWh} \end{aligned} \quad (5)$$

Considering the inverter efficiency, the value of RP_{Con} can be calculated as follows:

$$RP_{Con} = \frac{P_{Inv}^{max}}{\eta_{Inv}} \quad (6)$$

where, P_{Inv}^{max} is the maximum absorbed/injected power of the LAB/LIB. In addition, for a 10-year period, the values for BC_{SC} , BC_{Con} and BC_{Inv} are 15000 \$/kW, 50 \$/kWh [36] and 600 \$/kWh [37], respectively. The cost of HESS, which consists of an LAB/LIB stack, an SC, two converters and an inverter, can be calculated using (7):

$$\begin{aligned} C_{HESS} &= (RC_{BAT} \cdot BC_{BAT}) + (RC_{SC} \cdot BC_{SC}) + (RP_{BATCon} \cdot BC_{Con}) \\ &\quad + (RP_{SCCon} \cdot BC_{Con}) + (RP_{Inv} \cdot BC_{Inv}). \end{aligned} \quad (7)$$

where, RC_{SC} and BC_{SC} are the rated capacity (kWh) and base cost (\$/kWh) of the SC. RP_{SCCon} is the rated power (kW) of the bidirectional DC/DC converter, which is connected to the SC. As the utilization of LABs and LIB with SC in parallel results in 30% [23] and 19% [22] battery life extension. Therefore, considering base cost of 600 \$/kWh for an LAB stack and 1000 \$/kWh for an LIB stack without SC in parallel, the LAB and LIB with SC in parallel can perform 30% and 19% more life cycles, respectively.

Considering one discharge/charge cycle per day [35], the BC_{BAT} can be calculated for a 10-year period, as follows:

$$\begin{aligned} BC_{BAT}(LIB) &= \frac{1000\$}{6000life_cycles \times 1.3} \times 3650cycles \\ &\cong 561.54\$/kWh \end{aligned} \quad (8)$$

$$\begin{aligned} BC_{BAT}(LAB) &= \frac{600\$}{2000life_cycles \times 1.3} \times 3650cycles \\ &\cong 467.95\$/kWh \end{aligned} \quad (9)$$

The SC should provide the maximum required discharge (E_{maxDis}^{SC})/charge (E_{maxCha}^{SC}) energy in power shortage/surplus

cases to intercept frequency deviation. Therefore, it should have enough stored energy for injection in the most severe case of power shortage or enough uncharged capacity to absorb energy in the most severe case of surplus power. Considering the efficiencies of the converter and inverter, the required capacity of the SC stack can be calculated as follows:

$$E_{SC} = \frac{E_{maxDis}^{SC}}{\eta_{Inv} \cdot \eta_{Conv}} + (\eta_{Inv} \cdot \eta_{Conv} \cdot E_{maxCha}^{SC}) \quad (10)$$

The reference value of SC (SOC_{SC}^{ref}) should be carefully chosen so that the SC can provide both maximum discharged/charged energies. According to [38], the voltage of SCs can be decreased to 50% of their rated voltage, and consequently, they can only use 75% of their capacities to discharge/charge, which means 25% of its rated capacity should always be kept charged. On this basis, the SOC_{SC}^{ref} can be calculated using (11):

$$SOC_{SC}^{ref} = \frac{(E_{maxDis}^{SC} \times \eta_{dis,cha}) + (0.25 \times E_{SC})}{E_{SC}} \quad (11)$$

The values of RP_{Con} can be calculated based on the maximum power that is passed through the converter. Considering that the power of converter transmits through the inverter, and the inverter efficiency of the inverter is not considered in the simulations, the value of RP_{Con} can be calculated as follows:

$$RP_{Con} = \frac{P_{SC/LAB/LIB}^{max}}{\eta_{Inv}} \quad (12)$$

III. SIMULATION STUDIES

As the HESS and BESS are responsible for EMFC, the simulation studies are divided into two sections. First section deals with short-term frequency regulations, and the second section deals with long-term energy management. Using the results of these two sections, the sizing of components of LIBESS, LABESS, LISHESS and LASHESS will be carried out.

A. MG SPECIFICATIONS

Fig. 7 shows the MG network under study, which consists of a 0.4 kV distribution feeder connected to a 20 kV distribution network through a transformer. The network is the CIGRE distribution test system [4]. The MG contains a Solid-Oxide Fuel Cell (SOFC), a Microturbine (MT), a Diesel Generator (DEG), an ESS and two PV systems. The total installed capacity of DGs except PV systems are 72.2 kW. PV systems generate 9.75 kW and 2.25kW at the temperature of 35°C and solar radiation of 1000 W/m². The power rating of the SOFC is 10 kW. The power rating of the MT and DEG is 31.1 kVA. As the size of ESS elements including the LIB, LAB and SC has not been determined yet, their sizes are chosen large enough so that they can initially handle their duties in different scenarios of the islanded MG operation.

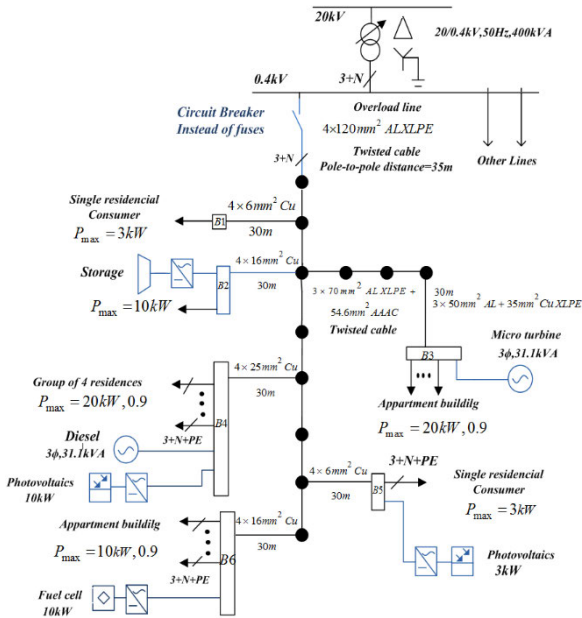


FIGURE 7. MG under study.

B. SIMULATION STUDIES FOR FREQUENCY REGULATION OF ISLANDED MG

Based on statistical data of [4], the most severe contingency that the MG may experiences is 20 kW power shortage after an unplanned islanding. The SOFC and MT model for frequency regulation studies can be found in [39] while the DEG model is adopted from model which is presented in [40]. For modelling the PV systems, the available PV models in Simulink/Matlab are used. The type of PV panels is Sun-power SPR-305E-WHT-D. The installed ESS whether HESS or BESS, is modeled based on the model and controllers presented in section 2.A. The power injection of the BESS whether using LAB or LIB is assumed to be similar. This assumption is also considered for the HESS. Therefore, the simulations are performed once with BESS and once with HESS.

1) FREQUENCY REGULATION USING BESS

In grid-connected mode, before islanding, the total demand and generation of the MG at specific time (5th second) are 64.1 kW and 44.1 kW, respectively. Therefore, 20 kW additional power is needed to compensate for the shortcomings in the islanded mode. Fig. 8 and 9, present the DGs power generation and MG frequency in islanded mode. It is obvious the frequency is dropped present to power shortage. To maintain the frequency deviation within a safe range, the BESS injects 28.61 kW immediately. In this way, the optimization algorithm (GA) tuned K1 at 57.334, considering the fast characteristics of the LIBESS in PFC, the frequency is intercepted at 49.501 Hz. However, this value is above the lower frequency limit (49.500 Hz). The slower-responding DGs, i.e., the SOFC, MT, and DEG gradually increase their power generation. The frequency returns to 50.000 Hz, and the LIBESS power returns to zero.

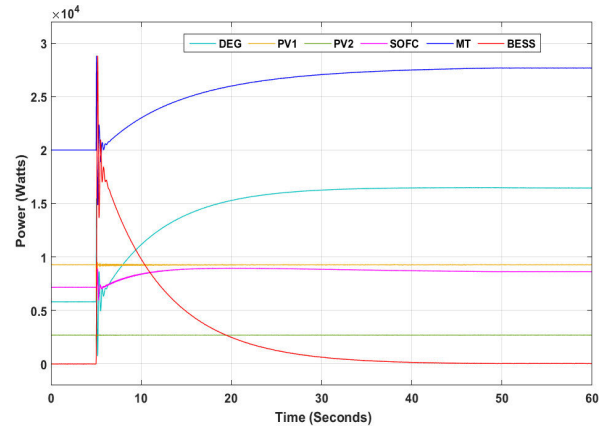


FIGURE 8. DGs power generation.

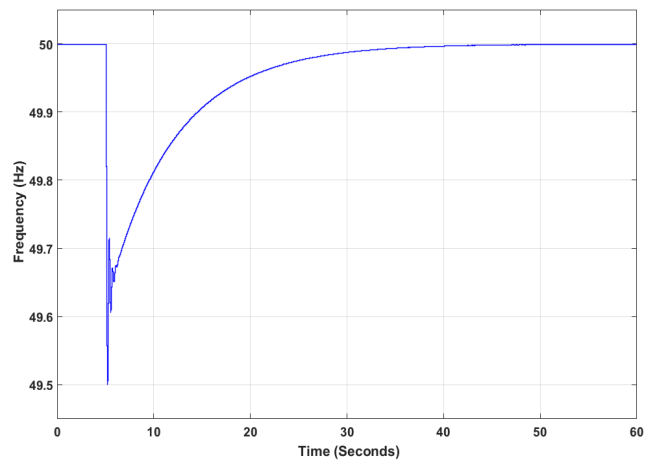


FIGURE 9. MG frequency response using BESS for PFC.

2) FREQUENCY REGULATION USING HESS

The Similar conditions for power shortage and it's disturbance as occurred in section 3.B.1 is applied in this section. Fig. 10 shows that after power shortage occurrence, the MG frequency drops. It can be seen in Fig. 11 that the SC and HESS provide a fast power injection with the peak power of 27.54 kW and 28.62 kW, respectively, and the frequency drop is intercepted at 49.501 Hz. For this purpose, K_1 is tuned at 55.19. The difference between the peak power of the SC and HESS is due to the slight contribution of the battery to PFC. The performance of the SOFC, DEG and MT restores frequency and the battery power to 50 Hz and 0 kW, respectively. The SC injects energy of 5.6331 Wh from the moment it responds to the frequency deviation till the moment its power becomes zero. The battery injects maximum power of 16.26 kW and total energy of 44.9901 Wh.

C. SIMULATION STUDIES FOR ENERGY MANAGEMENT OF ISLANDED MG

In this section, the size of the LAB/LIB is determined for the daily energy management. The installed capacity of DGs may not be enough to provide the MG demand during some periods such as the peak period. Therefore, the installation of an ESS for energy management and maintaining the balance

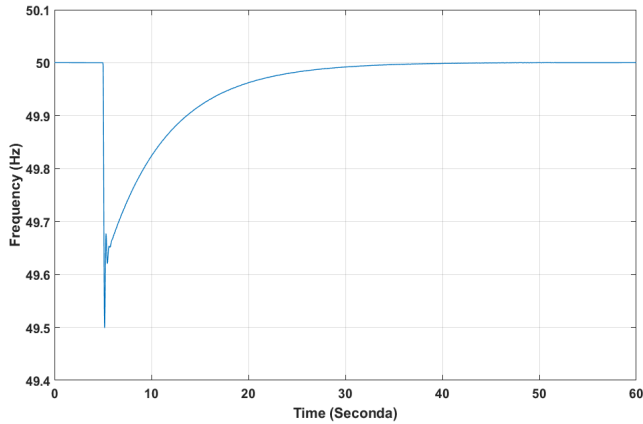


FIGURE 10. MG frequency response using HESS for PFC.

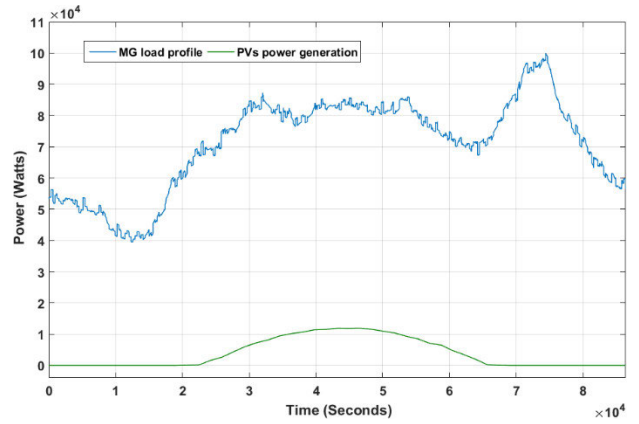


FIGURE 12. MG load profile and PVs power generation in mid-summer.

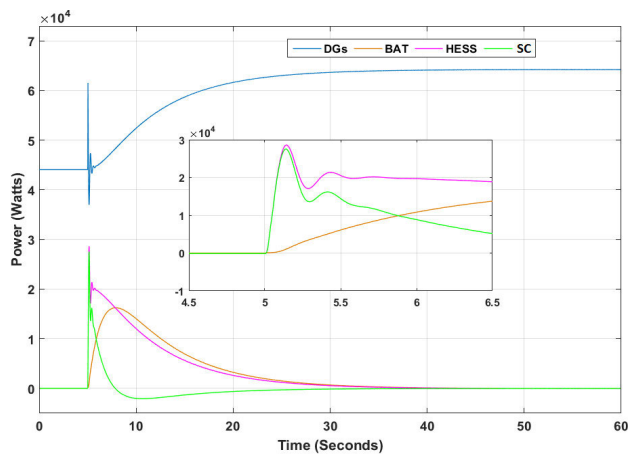


FIGURE 11. DGs power generation.

between demand and supply is necessary for the islanded MG. As the islanding occurrence time and its duration is not known, the battery is sized for the energy management of the islanded MG for the duration of one day islanding. The mid-summer day is taken as the worst case for energy management, given that if the BESS can manage power balance in this case, it can certainly be used for energy management in less severe cases. For longer durations, the same procedure, which is presented for one day energy management, can be used. The data of MG load profile is not available in [4], [41]. Therefore, the proposed profile of MG load in the mid-summer, which is shown in Fig. 12, is considered as the heaviest load profile that the MG experiences annually. The PVs power generation is also shown in this figure.

The model of the islanded MG and its components used for frequency regulation studies, cannot be used for energy management studies, because the simulation runtime is very long and the PC memory will overflow due to high volume of simulation data. Therefore, the models given in Figs. 6 and 7 are simulated in Simulink for energy management of the islanded MG with BESS and HESS, respectively. The MT and SOFC models presented in [42], and the model of DEG presented in [43] are used in the simulation studies for energy management.

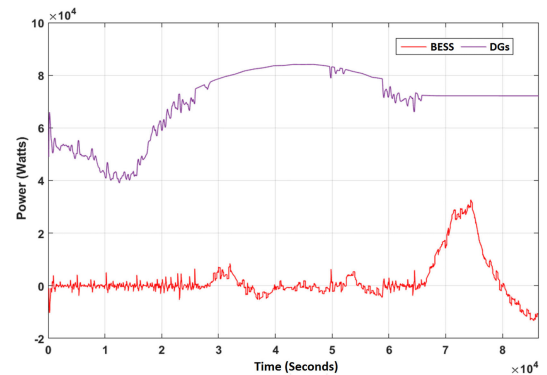


FIGURE 13. BESS power and total power generation of DGs.

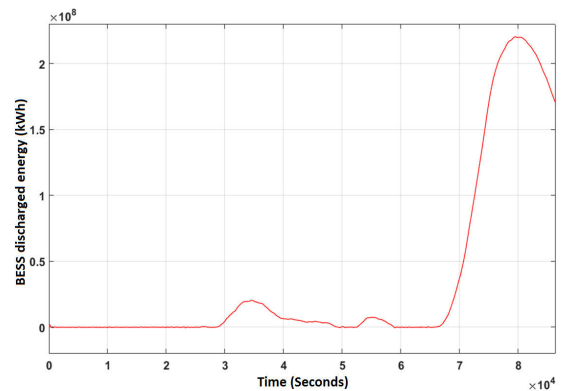


FIGURE 14. BESS Discharged energy.

1) ENERGY MANAGEMENT WITH BESS

Fig. 13 shows the total power generation of DGs and BESS power, and Fig. 14 shows the discharged energy of the BESS. It can be seen that during daily islanding in the mid-summer, the DGs mainly supply the loads. The BESS performs PFC and in peak-load periods that DGs reach their maximum capacity, it injects its stored energy to maintain balance between demand and supply. For this purpose, the BESS may go through several short and few long discharge/charge cycles. It should be noted that in peak-load periods, the DGs are controlled to generate their maximum power, so that the capacity of the BESS is used minimally, and

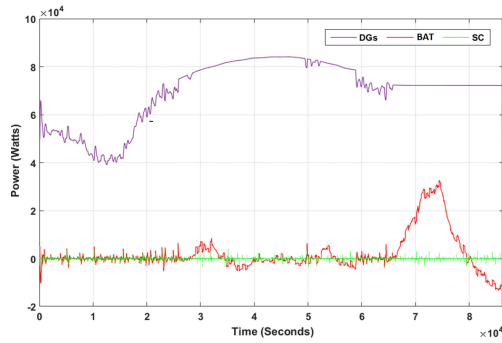


FIGURE 15. BESS power and total power generation of DGs.

the SOC of the battery (SOC_{BAT}) is maintained at (SOC_{BAT}^{ref}). Till $t = 65655$ sec, the DGs are successful in realizing these tasks. Till this moment, the total discharged/charged energy of the BESS is kept at zero, which means that the SOCLIB adjusts at SOC_{LIB}^{ref} . However, after this moment till $t = 79501$ sec, the MG load increases such that in order to maintain demand-supply balance, the BESS should also supply the demand while the DGs are generating their maximum power. It can be seen in Fig. 14 that the maximum discharged energy of the BESS in this period is much more than that of the previous discharge cycles. Therefore, the maximum discharged energy of the BESS in this period, determines the required capacity of the BESS for energy management, which is 61.2 kWh. In addition, the BESS maximum injected power is 32.66 kW.

2) ENERGY MANAGEMENT WITH HESS

Fig. 15 shows the total power generation of the DGs and the power of the SC and battery. The control strategy of the DGs in energy management of the islanded MG using the HESS is the same as energy management using BESS, except that the battery just responds to low-frequency components of the frequency deviations. The SC deals with high frequency components of the MG frequency.

As can be seen in Fig. 16, the discharged energy curve of the battery. The duration of the major discharge cycle of the battery is 13113 seconds, and the battery discharged energy during this cycle, is 61.19 kWh. The maximum injected power of the battery during its major discharge cycle is 32.66 kW. The maximum discharge energy of the SC in all discharge cycles is 0.42 Wh, and the maximum charge energy in all charge cycles is 0.46 Wh.

IV. COST EVALUATION OF LIBESS, LABESS, LISHESS AND LASHESS

The maximum discharged energy of the BESS in the EMFC studies is 61.2 kWh, and therefore, the required battery capacity can be calculated using (3):

$$RC_{BAT} = \frac{61.2}{0.9 \times 0.9} = 75.56kWh \quad (13)$$

Considering that the maximum absorbed/injected power of the LIB is 32.66 kW, the value of RP_{BATCon} is 32.29 kW, which is calculated using (6) and the value of RP_{Inv} is

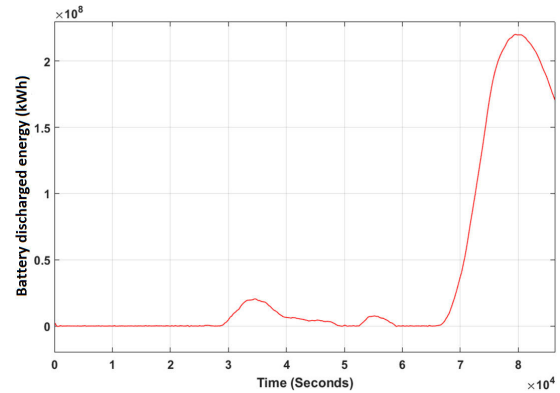


FIGURE 16. BESS Discharged energy.

32.66 kW. The cost of LIBESS and LABESS for a 10-year period can be calculated using (2), (4) and (5):

$$C_{LIBESS} = (36.29 \times 50) + (32.66 \times 600) + (75.56 \times 608.34) = 67376.67\$ \quad (14)$$

$$C_{LABESS} = (36.29 \times 50) + (32.66 \times 600) + (75.56 \times 730) = 76569.3\$ \quad (15)$$

In EMFC simulation studies with HESS, the maximum discharged energy of the battery is 61.19 kWh, and therefore, its required capacity can be calculated using (3):

$$RC_{BAT} = \frac{61.2}{0.9 \times 0.9} = 75.544kWh \quad (16)$$

The SC discharged energy of 5.6331 Wh in shortage power scenario, and charged energy of 4.1201 Wh in surplus scenario. Using (10), the required capacity of the SC stack can be calculated as follows:

$$E_{SC} = \left(\frac{5.6331}{0.9 \times 0.9} \right) + (4.1201 \times 0.9 \times 0.9) = 10.293Wh \quad (17)$$

Considering that the maximum absorbed/injected power of SC and battery are 27.54 kW and 32.66 kW, rated power of the inverter is equal to 32.66 kW. The values of RP_{SCCon} and RP_{BATCon} are 30.6 kW and 36.29 kW, which are calculated using (12). The cost of the LISHESS and LASHESS for a 10-year period can be achieved using (7)-(9):

$$C_{LISHESS} = (36.29 \times 50) + (30.6 \times 50) + (32.66 \times 600) + (75.56 \times 467.95) + (10.293 \times 10^{-3} \times 15000) = 58445.71\$ \quad (18)$$

$$C_{LASHESS} = (36.29 \times 50) + (30.6 \times 50) + (32.66 \times 600) + (75.56 \times 467.95) + (10.293 \times 10^{-3} \times 15000) = 65515.875\$ \quad (19)$$

It can be seen that for a 10-year period operation in islanded MG, the HESSs impose less cost than BESSs. The LISHESS is cheaper (almost 11%) than LASHESS. Also, the cost of LIBESS is much less than that of LABESS. It seems that hybridizing the battery technologies with the SC results in considerable cost reduction and LIB is more cost-efficient than LAB.

V. CONCLUSION

In recent years, the hybridization of the LABs and LIBs with the SCs has been proposed to prolong their life cycles and hence reduce operational cost. Therefore, in this paper, the cost effectiveness of their hybridization was investigated for islanded MG applications. For this purpose, an EMFC scheme was proposed that maintained the demand-supply balance and also kept the frequency within safe operational limits. In addition, the coordination of DGs and ESSs minimized the required capacities of the LAB and LIB for the energy management of the islanded MG. Using the simulation results and the proposed procedure for sizing and cost evaluation, their costs were determined. It was shown that the HESSs impose less cost than BESSs. The LISHES is cheaper (almost 11%) than LASHES, which is mostly because the cost per life cycles of the LIB is much less than that of the LAB. For the same reason, the cost of LIBESS is much less than that of LABESS. It can be summarized that hybridizing the battery technologies with the SC results in considerable cost reduction and LIB is more cost-efficient than LAB.

Although, the hybridization of LIB and LAB with SCs are more common than other HESS, the hybridization of other ESS elements with each other has also been proposed like superconducting magnetic energy storage-battery HESS. For future work, it would be interesting to also perform a techno-economic analysis between their single utilization and their hybrid utilization for ESS applications. For this purpose, the same approach which was used in this paper for LIBESS, LABESS, LISHES and LASHES, can be implemented.

REFERENCES

- [1] M. B. Sanjareh, M. H. Nazari, G. B. Gharehpetian, and S. H. Hos-Seanian, "New approach for sizing of overloaded-capable battery for microgrid frequency control using cooperation of PVs, BESS and smart lighting loads," *J. Intell. Fuzzy Syst.*, pp. 1–15, Jul. 2020.
- [2] A. Khodadadi, P. Hasanpor Divshali, M. H. Nazari, and S. H. Hosseinian, "Small-signal stability improvement of an islanded microgrid with electronically-interfaced distributed energy resources in the presence of parametric uncertainties," *Electr. Power Syst. Res.*, vol. 160, pp. 151–162, Jul. 2018.
- [3] F. Katiraei and M. R. Iravani, "Power management strategies for a microgrid with multiple distributed generation units," *IEEE Trans. Power Syst.*, vol. 21, no. 4, pp. 1821–1831, Nov. 2006.
- [4] M. Bagheri-Sanjareh, M. H. Nazari, and G. B. Gharehpetian, "A novel and optimal battery sizing procedure based on MG frequency security criterion using coordinated application of BESS, LED lighting loads, and photovoltaic systems," *IEEE Access*, vol. 8, pp. 95345–95359, 2020.
- [5] A. Krkoleva Mateska, V. Borozan, P. Krstevski, and R. Taleski, "Controlable load operation in microgrids using control scheme based on gossip algorithm," *Appl. Energy*, vol. 210, pp. 1336–1346, Jan. 2018.
- [6] Y. Karimi, H. Oraee, M. S. Golsorkhi, and J. M. Guerrero, "Decentralized method for load sharing and power management in a PV/battery hybrid source islanded microgrid," *IEEE Trans. Power Electron.*, vol. 32, no. 5, pp. 3525–3535, May 2017.
- [7] M. Bagheri-Sanjareh and M. H. Nazari, "Coordination of energy storage system, PVs and smart lighting loads to reduce required battery size for improving frequency response of islanded microgrid," *Sustain. Energy, Grids Netw.*, vol. 22, Jun. 2020, Art. no. 100357.
- [8] M. Bagheri Sanjareh, M. H. Nazari, and S. H. Hosseinian, "A novel strategy for frequency control of islanded greenhouse with cooperative usage of BESS and LED lighting loads," *Electr. Eng.*, pp. 1–13, Aug. 2020.
- [9] S. Dhundhara, Y. P. Verma, and A. Williams, "Techno-economic analysis of the lithium-ion and lead-acid battery in microgrid systems," *Energy Convers. Manage.*, vol. 177, pp. 122–142, Dec. 2018.
- [10] D. Tenfen, E. C. Finardi, F. Wurtz, and B. Delinchant, "Lithium-ion battery modelling for the energy management problem of microgrids," *IET Gener. Transmiss. Distrib.*, vol. 10, no. 3, pp. 576–584, Feb. 2016.
- [11] T. H. Mehr, M. A. S. Masoum, and N. Jabalameli, "Grid-connected lithium-ion battery energy storage system for load leveling and peak shaving," in *Proc. Australas. Univ. Power Eng. Conf. (AUPEC)*, Sep. 2013, pp. 1–6.
- [12] N. Mendis, K. M. Muttaqi, and S. Perera, "Management of low-and high-frequency power components in demand-generation fluctuations of a DFIG-based wind-dominated RAPS system using hybrid energy storage," *IEEE Trans. Ind. Appl.*, vol. 50, no. 3, pp. 2258–2268, May 2014.
- [13] W. Jing, C. H. Lai, W. S. H. Wong, and M. L. D. Wong, "A comprehensive study of battery-supercapacitor hybrid energy storage system for standalone PV power system in rural electrification," *Appl. Energy*, vol. 224, pp. 340–356, Aug. 2018.
- [14] K. O. Ourelidis, E. A. Bakirtzis, and C. S. Demoulias, "Frequency-based control of islanded microgrid with renewable energy sources and energy storage," *J. Mod. Power Syst. Clean Energy*, vol. 4, no. 1, pp. 54–62, Jan. 2016.
- [15] S. Augustine, M. K. Mishra, and N. Lakshminarasamma, "A unified control scheme for a standalone solar-PV low voltage DC microgrid system with HESS," *IEEE J. Emerg. Sel. Topics Power Electron.*, vol. 8, no. 2, pp. 1351–1360, Jun. 2020.
- [16] L. Zhang, X. Ye, X. Xia, and F. Barzegar, "A real-time energy management and speed controller for an electric vehicle powered by a hybrid energy storage system," *IEEE Trans. Ind. Informat.*, vol. 16, no. 10, pp. 6272–6280, Oct. 2020.
- [17] W. Liu, W. Gu, X. Yuan, and K. Zhang, "Fully distributed control to coordinate charging efficiencies for energy storage systems," *J. Mod. Power Syst. Clean Energy*, vol. 6, no. 5, pp. 1015–1024, Sep. 2018.
- [18] M. F. Zia, E. Elbouchikhi, and M. Benbouzid, "Microgrids energy management systems: A critical review on methods, solutions, and prospects," *Appl. Energy*, vol. 222, pp. 1033–1055, Jul. 2018.
- [19] X. Li, Z. Li, L. Guo, J. Zhu, Y. Wang, and C. Wang, "Enhanced dynamic stability control for low-inertia hybrid AC/DC microgrid with distributed energy storage systems," *IEEE Access*, vol. 7, pp. 91234–91242, 2019.
- [20] W. Jing, C. H. Lai, D. K. X. Ling, W. S. H. Wong, and M. L. D. Wong, "Battery lifetime enhancement via smart hybrid energy storage plug-in module in standalone photovoltaic power system," *J. Energy Storage*, vol. 21, pp. 586–598, Feb. 2019.
- [21] S. Wen, S. Wang, G. Liu, and R. Liu, "Energy management and coordinated control strategy of PV/HES AC microgrid during islanded operation," *IEEE Access*, vol. 7, pp. 4432–4441, 2019.
- [22] A. M. Gee, F. V. P. Robinson, and R. W. Dunn, "Analysis of battery lifetime extension in a small-scale wind-energy system using supercapacitors," *IEEE Trans. Energy Convers.*, vol. 28, no. 1, pp. 24–33, Mar. 2013.
- [23] N. Omar, J. Van Mierlo, B. Verbrugge, and P. Van den Bossche, "Power and life enhancement of battery-electrical double layer capacitor for hybrid electric and charge-depleting plug-in vehicle applications," *Electrochimica Acta*, vol. 55, no. 25, pp. 7524–7531, Oct. 2010.
- [24] I. J. Cohen, D. A. Wetz, J. M. Heinzel, and Q. Dong, "Design and characterization of an actively controlled hybrid energy storage module for high-rate directed energy applications," *IEEE Trans. Plasma Sci.*, vol. 43, no. 5, pp. 1427–1433, May 2015.
- [25] R. Carter, A. Cruden, and P. J. Hall, "Optimizing for efficiency or battery life in a battery/supercapacitor electric vehicle," *IEEE Trans. Veh. Technol.*, vol. 61, no. 4, pp. 1526–1533, May 2012.
- [26] T. Kerdphol, K. Fuji, Y. Mitani, M. Watanabe, and Y. Qudaih, "Optimization of a battery energy storage system using particle swarm optimization for stand-alone microgrids," *Int. J. Electr. Power Energy Syst.*, vol. 81, pp. 32–39, Oct. 2016.
- [27] T. Kerdphol, Y. Qudaih, and Y. Mitani, "Optimum battery energy storage system using PSO considering dynamic demand response for microgrids," *Int. J. Electr. Power Energy Syst.*, vol. 83, pp. 58–66, Dec. 2016.
- [28] T. A. Jumani, M. W. Mustafa, M. M. Rased, N. H. Mirjat, Z. H. Leghari, and M. S. Saeed, "Optimal voltage and frequency control of an islanded microgrid using grasshopper optimization algorithm," *Energies*, vol. 11, no. 11, p. 3191, Nov. 2018.
- [29] M. H. Nazari, S. H. Hosseinian, and E. Azad-farsani, "A multi-objective LMP pricing strategy in distribution networks based on MOGA algorithm," *J. Intell. Fuzzy Syst.*, pp. 1–12, May 2019.

- [30] M. H. Nazari, S. H. Hosseinian, E. Azad-farsani, and D. Faramarzi, "An incentive-based policy on reduction of GHG emissions and loss minimization using adaptive group search multi-objective optimization algorithm," *Sci. Iran.*, pp. 1–35, Sep. 2019.
- [31] M. H. Nazari, S. H. Hosseinian, and E. Azad-Farsani, "Shapley value-based techno-economic framework for harmonic and loss mitigation," *IEEE Access*, vol. 7, pp. 119576–119592, Aug. 2019.
- [32] J. Patel, H. Chandwani, V. Patel, and H. Lakhani, "Bi-directional DC-DC converter for battery charging—Discharging applications using buck-boost switch," in *Proc. IEEE Students' Conf. Elect., Electron. Comput. Sci.*, Mar. 2012, pp. 1–4, doi: [10.1109/SCEECS.2012.6184993](https://doi.org/10.1109/SCEECS.2012.6184993).
- [33] Z. Xie, L. Du, X. Lv, Q. Wang, J. Huang, T. Fu, and S. Li, "Evaluation and analysis of battery technologies applied to grid-level energy storage systems based on rough set theory," *Trans. Tianjin Univ.*, vol. 26, pp. 228–235, Feb. 2020.
- [34] G. J. May, A. Davidson, and B. Monahov, "Lead batteries for utility energy storage: A review," *J. Energy Storage*, vol. 15, pp. 145–157, Feb. 2018.
- [35] S.-J. Lee, J.-H. Kim, C.-H. Kim, S.-K. Kim, E.-S. Kim, D.-U. Kim, K. K. Mehmood, and S. U. Khan, "Coordinated control algorithm for distributed battery energy storage systems for mitigating voltage and frequency deviations," *IEEE Trans. Smart Grid*, vol. 7, no. 3, pp. 1713–1722, May 2016.
- [36] M. Masih-Tehrani, M. R. H. Yazdi, V. Esfahanian, M. Dahmardeh, and H. Nehzati, "Wavelet-based power management for hybrid energy storage system," *J. Mod. Power Syst. Clean Energy*, vol. 7, no. 4, pp. 779–790, Jul. 2019.
- [37] B. Glasgo, I. L. Azevedo, and C. Hendrickson, "How much electricity can we save by using direct current circuits in homes? Understanding the potential for electricity savings and assessing feasibility of a transition towards DC powered buildings," *Appl. Energy*, vol. 180, pp. 66–75, Oct. 2016.
- [38] A. Lahyani, P. Venet, A. Guermazi, and A. Troudi, "Battery/supercapacitors combination in uninterruptible power supply (UPS)," *IEEE Trans. Power Electron.*, vol. 28, no. 4, pp. 1509–1522, Apr. 2013.
- [39] Y. Zhu and K. Tomsovic, "Development of models for analyzing the load-following performance of microturbines and fuel cells," *Electr. Power Syst. Res.*, vol. 62, no. 1, pp. 1–11, May 2002.
- [40] V. Friedel, "Modeling and simulation of a hybrid wind-diesel microgrid," KTH Roy. Inst. Technol., Stockholm, Sweden, Tech. Rep., 2009.
- [41] M. B. Sanjareh, M. H. Nazari, G. B. Gharehpetian, and S. M. S. Ghiasi, "A novel strategy for optimal battery sizing based on MG frequency security criterion," in *Proc. Int. Power Syst. Conf. (PSC)*, Dec. 2019, pp. 716–722.
- [42] R. M. Kamel and B. Kermanshahi, "Design and implementation of models for analyzing the dynamic performance of distributed generators in the micro grid part I: Micro turbine and solid oxide fuel cell," *Sci. Iran.*, vol. 17, no. 1, pp. 47–58, 2010.
- [43] Y.-S. Kim, E.-S. Kim, and S.-I. Moon, "Frequency and voltage control strategy of standalone microgrids with high penetration of intermittent renewable generation systems," *IEEE Trans. Power Syst.*, vol. 31, no. 1, pp. 718–728, Jan. 2016.



MARYAM TORKASHVAND was born in Tehran, Iran, in 1995. She received the bachelor's degree in electrical engineering, in 2017. She is currently pursuing the master's degree in electrical engineering with the Islamic Azad University Science and Research Branch, Tehran.



ABOLFAZL KHODADADI was born in Arak, Iran, in 1993. He received the bachelor's degree in electrical engineering from the Isfahan University of Technology, Tehran, in 2016, and the master's degree in power engineering from the Amirkabir University of Technology, Tehran, Iran, in 2018. He is currently pursuing the Ph.D. degree in power electrical engineering with the KTH Royal Institute of Technology, Stockholm, Sweden.



MEHRDAD BAGHERI SANJAREH was born in Iran, in 1993. He received the bachelor's degree in electrical engineering from Shahed University, Tehran, in 2014, and the master's degree in power engineering from Shahid Beheshti University.



MUHAMMAD H. NAZARY was born in Iran, in 1988. He received the bachelor's degree in electrical engineering from Shahed University, Tehran, Iran, in 2011, the master's degree in power engineering from the Sharif University of Technology, in 2013, and the Ph.D. degree in power system engineering from the Tehran polytechnic, Tehran, in 2020. He is currently involved in the Department of Electrical Engineering, Amirkabir University of Technology, as a Postdoctoral Researcher.

...